Polyolefin Nanocomposites with Improved Performance

Ton-That, Minh-Tan; Bureau, Martin N.; Perrin-Sarazin, Florence; Denault, Johanne; Cole, Kenneth C.

Publisher's version / Version de l'éditeur:

Proceedings. The 63rd Annual Technical Conference (ANTEC 2005), 4, pp. 191-195, 2005

POLYOLEFIN NANOCOMPOSITES WITH IMPROVED PERFORMANCE

Minh-Tan Ton-That, Martin N Bureau, Florence Perrin-Sarazin, Johanne Denault, and Kenneth C Cole
Industrial Materials Institute / National Research Council Canada
75 De Mortagne Blvd., Boucherville, Québec, Canada J4B 6Y4

Abstract

The preparation of nanoclay-reinforced polyolefin nanocomposites by means of melt processing was investigated. Different types of compatibilizers based on glycidyl-methacrylate-grafted polypropylene (PP) have been developed for the formation of PP nanocomposites. Different formulations and processing conditions were used to optimize the chemical interaction between the organic and inorganic phases (i.e. the polymer matrix and the clay) in order to maximize the clay dispersion and the clay-matrix interface. Fourier transform infrared spectroscopy (FT-IR), X-ray diffraction (XRD), scanning electron microscopy (SEM), and transmission electron microscopy (TEM) were used to study the chemical interactions between the polymer and the organoclay as well as the dispersion of the organoclays and the nanocomposite morphology. Various properties of the resulting nanocomposites, such as the physicochemical properties, the mechanical properties (including fracture toughness from essential work of fracture), and the thermal stability, were also evaluated. The relationship between formulation, structure, and performance is discussed.

Introduction

Nanocomposites based on nano-layered silicates have attracted much attention during the past ten years because of their low cost, their ready availability, and their non-isometric structure derived from a high aspect ratio, which can maximize the reinforcing effect in terms of mechanical, thermal, and barrier properties (1). In comparison with the pure polymer or conventional (microscale) composites, the presence of nano-layered silicates in the polymer matrix can significantly increase moduli, strength, and heat resistance, and decrease gas permeability and flammability. However, good dispersion of nanoclay in the polymer matrix and a good interface between the two phases are essential to achieve the improvements mentioned. Owing to the natural incompatibility between the hydrophilic clay and the hydrophobic matrices (especially polyolefins), these characteristics are not always easy to achieve. In addition, the clay layers tend to bond strongly together, which makes the dispersion of the clay into the polymer matrix more difficult.

The approaches used to overcome these problems include modification of the clay surface by organo-intercalant to reduce the interaction between the clay platelets while at the same time making them more compatible with the polymer matrix (1-3), or modification of the polyolefin matrix by incorporating a more hydrophilic coupling agent to make it more compatible with the clay (2-6), or a combination of both. Maleic anhydride (MA) or acrylic acid (AA) grafted PP (MAgPP, AAgPP, respectively) have been the most popular coupling agents for the formation of PP nanocomposites. Because of the high cost of the coupling agents, only a limited amount should be used. As a result, full dispersion of nanoclays (so-called exfoliation) in PP by melt blending has remained difficult to achieve; the usual result is instead rather poor intercalation, where the clay layers remain in stacks with limited expanded galleries. It is necessary to search for an alternative coupling agent in order to improve the dispersion and interface. Epoxide groups are well known to be reactive, and can react with different functional groups, including hydroxyl, amine, amide, etc. The use of epoxide based coupling agents, for example glycidyl-methacrylate-grafted PPs (GMAgPPs), for the formation of PO nanocomposites has not been explored thoroughly.

The objective of this work is to improve the compatibilization between the clays and the PP matrix in order to optimize the dispersion and the interface of PP nanocomposites, and hence improve on their performance. This paper will present the effect of GMAgPP coupling agent on the structure and then the performance of PP nanocomposites.

Experimental

Materials

Polypropylene 6100SM from Montell was used as the matrix. Two types of conventional maleic-anhydride-grafted polypropylene (MAgPP) were used as coupling agents, one with low molecular weight but high graft content (Eastman Chemicals Epolene E43, designated as MA1), and one with high molecular weight but low graft content (Crompton Corp. Polybond 3150, designated as MA2). GMAgPP (designated as GMA) was prepared as described elsewhere (7). The amounts of grafted GMA and styrene were 0.43 and 0.27 wt%, respectively. The weight average molecular weights of the MA1, MA2 and GMA are respectively 9,000, 330,000 and 390,000. The amounts of grafted MA in MA1 and MA2 was ~4.8 and 1wt%, respectively.

Cloisite 15A, a commercially available nanoclay based on montmorillonite from Southern Clay Products, was used in this study. The clay surface was modified with dimethyl dihydrogenated tallow onium ion with an excess amount of roughly 12%. The gallery distance determined by X-ray diffraction analysis for the Cloisite 15A was 3.3 nm.

Nanocomposite Preparation

The nanocomposite samples were prepared in a twin-screw extruder (TSE) at temperatures not exceeding 200°C. The clay and coupling agent content were kept constant at 4 wt% and 8 wt% respectively. A complete description of the nanocomposites prepared in this study is given in Table 1. Finally, samples for testing mechanical properties were processed by injection molding. All the raw materials and also the nanocomposites were dried at 120°C for 4 h prior to processing in order to minimize degradation.

Characterization

To evaluate the dispersion of the nanoclay in the polymer matrix, X-ray diffraction patterns were obtained from compression-molded samples by means of a Bruker Discover 8 diffractometer operating at 40 kV and 40 mA with CuKα radiation. A Hitachi H9000 TEM was used to observe the clay intercalation/exfoliation. Infrared spectroscopy was used to obtain chemical information; spectra were measured on a Nicolet Magna 860 Fourier transform instrument at a resolution of 4 cm^{-1}. A Leitz optical microscope coupled with Mettler hotstage and a Perkin Elmer Pyris DSC were used to study the crystallization behavior. Tensile and flexural properties were determined according to ASTM test methods D638 and D790, respectively, using an Instron 5500R machine. The fracture toughness was evaluated according to the essential work of fracture (EWF) method as described elsewhere (8).

The EWF method consists in measuring the area under the load-displacement curve of specimens containing a severe stress concentration zone designed to obtain a fully developed plastic zone in the fracture region. The specific work of fracture w_f can be expressed as the following linear function:

$$w_t = w_e + \beta w_p \cdot l \qquad (1)$$

where w_e and $\beta \cdot w_p$ are the essential and non-essential work of fracture, respectively. The value of w_e corresponds to the quantitative measurement of the fracture toughness, the intrinsic resistance of a material to the initiation of a critical defect leading to fracture. The value of $\beta \cdot w_p$ corresponds to the quantitative measurement of plastic work dissipation, similar to the ductility of a material.

Results and Discussion

The clay d-spacing in the PP matrix with and without the inclusion of coupling agent as measured by X-ray is shown in Table 2. Cloisite 15A has been treated with excess intercalant with the intention of facilitating the dispersion. In the absence of coupling agent, the d-spacing decreases, indicating that the unbound intercalant has left the clay galleries. It is clear that the presence of coupling agents significantly improves the dispersion of the nanoclay although the extent depends on the type of coupling agent. The MA1 with shorter molecular weight and higher grafting amount provides a slightly greater d-spacing, while MA2 with high molecular weight and low grafting amount gives the smallest d-spacing among the three, although the difference in the absolute d-spacing is not very large. However, comparing the d-spacing of these samples with that of the sample prepared without coupling agent (15A) leads to a more meaningful observation. The increase observed relates to the diffusion of coupling agent into the clay gallery, and therefore better dispersion and better interfacial interaction, which is absent in the sample without coupling agent. The MA1 leads to greater expansion in the clay gallery distance; this is probably due to its high grafting amount and its smaller molecular weight, which improve respectively the affinity with the clay and the chain mobility for the diffusion. The MA2, which has higher grafting amount and lower molecular weight than GMA, should lead to better intercalation, but the results are quite the opposite. This may be explained by the difference in chemistry and structure between them. GMA has been co-grafted with styrene, which is believed to form a short chain "copolymer-like" structure at the grafting portion, while MA has been directly attached on the PP chain. In addition, the high reactivity of the epoxy group in GMA is also another reason.

Clays can be considered to be fully exfoliated only if sufficient matrix diffuses into the clay galleries to eliminate a strong interaction between the clay layers, which corresponds to a spacing of approximately 7 nm. Based on this information, to achieve full exfoliation the concentration of the inorganic clay in the nanocomposite should not be greater than 2 wt%. In the nanocomposites studied, the clay concentration exceeds this critical value, so full exfoliation cannot be expected. TEM observation demonstrates that in the presence of coupling agent, in addition to intercalation, partial exfoliation also occurred at different levels, depending on the type of coupling agent. MA2 provides better exfoliation than MA1, while Figure 1 shows that GMA allows better exfoliation than MA2. The clay in GMA-15A shows smaller stacks with more evidence of single, double and triple stacks than in MA2-15A. This again confirms an advantage of the GMA over the MA in terms of dispersion.

To obtain more information on the chemistry of the nanocomposites, transmission infrared spectra were

run on thin films prepared by rapid hot pressing. The spectra are complex because they consist of overlapping peaks from four materials—PP, clay, intercalant, and coupling agent. As a result, no clear conclusions could be drawn.

Optical microscope observations were also made for the PP, 15A, MA1-15A, MA2-15A and GMA-15A. It is very interesting to find that the crystallization characteristics of the PP matrix remain more or less the same in all samples; they are characterized by well defined spherulites, except for the GMA-15A. However, the spherulite size decreased significantly with the presence of clays and coupling agents. As demonstrated in Figure 2, the GMA-15A produces a very fine crystalline structure, in which the spherulite structure cannot be seen even by SEM on samples which have been chemically attacked. In addition, the crystallization took place earlier and then progressed very fast compared to all the others. It can be concluded that the GMA has generated a high nucleating efficiency for the crystallization of the PP. It is still unclear whether this is due to by-products of the grafting process or to the GMA itself.

Furthermore, Table 3 indicates that the presence of clay and coupling agent seems to reduce the degree of crystallinity to different extents, depending on the formulation. The nanocomposite containing GMA leads to a higher degree of crystallinity compared to MA1 and MA2. This confirms the nucleating effect of the GMA shown by optical microscopy.

The tensile and flexural properties of these nanocomposites are presented in Figures 3 and 4. In the absence of coupling agent, the clays are poorly dispersed and remain in large aggregates. As a result, the clay reinforcing effect is very limited. Owing to much better dispersion and probably a better interface, the MA1 and MA2 significantly improve the strength and stiffness of the nanocomposites in both flexion and tension. However, the GMA leads to even better performance. The modulus improvement should relate directly to the better dispersion, while the strength improvement should be due to a better clay-matrix interface in this sample. In addition, its distinctive crystalline morphology may also contribute to this exceptional improvement. For example, the fine crystals in this sample are likely to have a negligible impact on the clay orientation during crystallization. This means that the clay can better retain the preferred orientation generated by injection molding. Furthermore, its fine crystalline structure should benefit from a low level of imperfection, which has a significant impact on the material strength.

Another advantage of GMA was also observed in terms of ductility and toughness. The typical stress-strain curves shown in Figure 5 for MA1-15A and GMA-15A indicate a very large difference in elongation at break; GMA-15A was found to show very high ductility in comparison to both MA1-15A and MA2-15A. This resulted in stable necking extension to the complete specimen for GMA-15A instead of the rapid break after yield seen for MA1-15A and MA2-15A. This behavior was confirmed by the fracture toughness measurements reported in Figure 6. This figure illustrates that the fracture curves of 15A, MA1-15A, and MA2-15A lie considerably below the fracture curve of PP (although their slopes are different), whereas the fracture curve of GMA-15A is parallel to and above the fracture curve of PP. These results are presented numerically in Table 4, which indicates that the fracture toughness of 15A, MA1-15A, and MA2-15A is 60 to 75% below that of PP, while the fracture toughness of GMA-15A is 33% above it. It also shows that the plastic work dissipation values of these materials varies considerably. As reported previously for PP-based nanocomposites (9), this plastic work dissipation is affected by matrix-particle coupling, particle size dispersion, and the matrix properties. The values of plastic work dissipation in Table 4 suggest that in 15A the plastic zone is considerably larger than in the other materials, as a result of the larger clay particles acting as void initiation sites (7) in a soft PP matrix. This contrasts with the plastic work dissipation values of MA1-15A, MA2-15A, and GMA-15A, which are considerably lower than for 15A. It is difficult to draw conclusions, however, on the origin(s) of the differences between MA1-15A, MA2-15A and GMA-15A.

The EWF values nonetheless indicate that only GMA-15A presents a fracture toughness superior to that of PP, while 15A, MA1-15A, and MA2-15A present fracture toughness values significantly reduced with respect to PP. This improved fracture toughness is the consequence of both effective particle-matrix coupling and very good particle dispersion (intercalation/exfoliation). It cannot be ruled out either that the effect of GMA on the crystalline morphology of PP in GMA-15A may also contribute to its improved fracture toughness.

Conclusions

GMAgPP provides much better dispersion and interfacial interaction compared to MAgPP. In addition it modifies the crystallization morphology of PP to form a very fine crystalline structure. As a result, the nanocomposites based on GMAgPP possess superior strength, stiffness, and ductility.

Moreover, while 15A, MA1-15A, and MA2-15A present low ductility and low fracture toughness, GMA-15A shows high ductility and improved fracture toughness (+33%), indicating effective particle-matrix coupling and very good particle dispersion (intercalation/exfoliation).

Acknowledgements

The authors would like to thank Claudine Roux, Michel Champagne, and Michel Huneault for providing the GMA samples. The technical contributions of Mr. Yves Simard, Mrs. Manon Plourde and Mrs. Chantal Coulombe are also gratefully acknowledged.

KEYWORDS: Polypropylene, Nanocomposites, Coupling Agents, Microstructure, Crystallinity, Particle Dispersion, Mechanical Properties, Fracture Toughness

References

1. L. A. Utracki and M. R. Kamal, *Arabian J. Sci. Eng.* 2002, **27**, 43.
2. A. Usuki, M. Kato, A. Okada, and T. Kurauchi, *J. Appl. Polym. Sci.* 1997, **63**, 137.
3. M. Kawasumi, N. Hasegawa, M. Kato, A. Usuki, and A. Okada, *Macromolecules* 1997, **30**, 6333.
4. P. Reichert, H. Nitz, S. Klinke, R. Brandsch, R. Thomann, and R. Mülhaupt, *Macromol. Mater. Eng.* 2000, **275**, 8.
5. N. Hasegawa, H. Okamoto, M. Kato, and A. Usuki, *J. Appl. Polym. Sci.* 2000, **78**, 1918.
6. H. Wang, C. Zeng, M. Elkovitch, L. J. Lee, and K. W. Koelling, *Polym. Eng. Sci.* 2001, **41**, 2036.
7. C. Roux, M. Champagne, and M. Huneault, *Proc. SPE ANTEC* (2000).
8. M. N. Bureau, F. Perrin-Sarazin, and M.-T. Ton-That, *Proc. SPE ANTEC* (2004).
9. M.-T. Ton-That., F. Perrin-Sarazin and M. N. Bureau, *Polym. Eng. Sci.* 2004, 44 (7), 1212.

Table 1. Description of the nanocomposites.

Designation	Clay type	Coupling agent type
0	None	None
15A	15A	None
MA1-15A	15A	E43
MA2-15A	15A	PB3150
GMA-15A	15A	GMA

Table 2. Gallery spacing of the clays in the nanocomposites.

Sample	d-spacing (nm)
Cloisite 15A	3.39
15A	2.88
MA1-15A	3.69
MA2-15A	3.21
GMA-15A	3.51

Table 3. Degree of crystallinity of PP and its nanocomposites.

Sample	T_c (°C)	Crystallinity (%)
PP	118	68.7
15A	126	67.8
MA1-15A	120	59.1
MA2-15A	123	61.36
GMA-15A	128	67.4

Table 4. Work of fracture and plastic dissipation of the PP and its nanocomposites.

Sample	EWF (kJ/m^2)	Plastic Dissipation (MJ/m^3)
PP	14.9	0.38
15A	3.8	1.29
MA1-15A	6.2	0.20
MA2-15A	6.0	0.66
GMA-15A	19.8	0.37

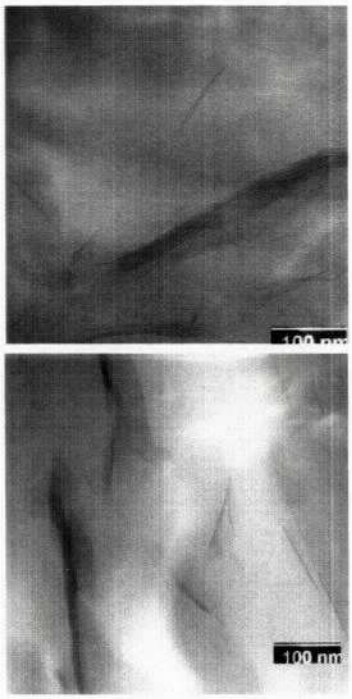

Fig 1. TEM images of (a) MA2-15A and (b) GMA-15A.

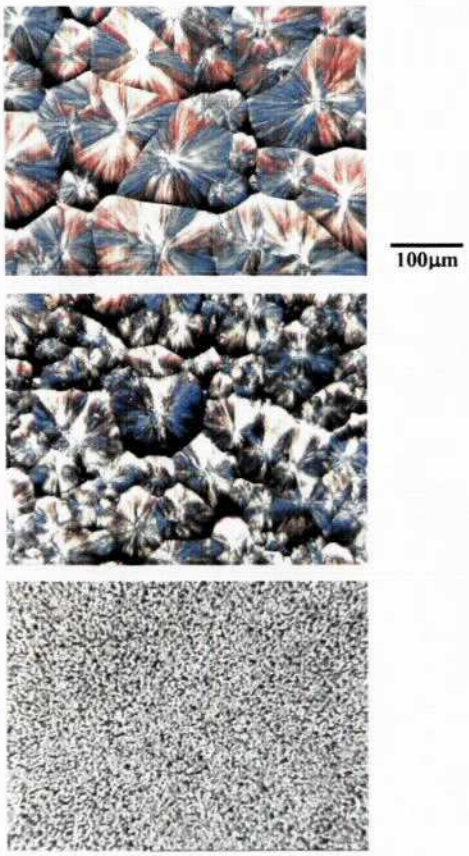

Fig. 2. Optical microscope observation of: (a) the PP matrix, (b) MA1-15A and (c) GMA-15A.

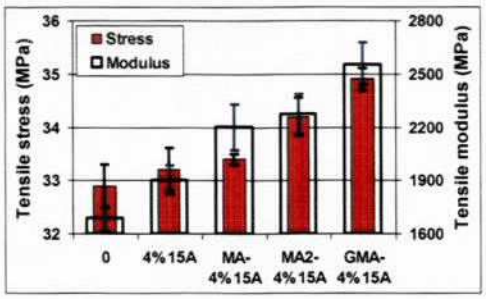

Fig. 3. Tensile properties of the PP and its nanocomposites.

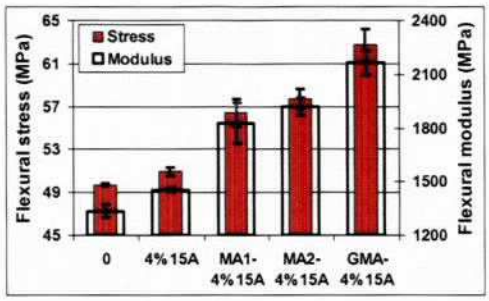

Fig. 4. Flexural properties of the PP and its nanocomposites.

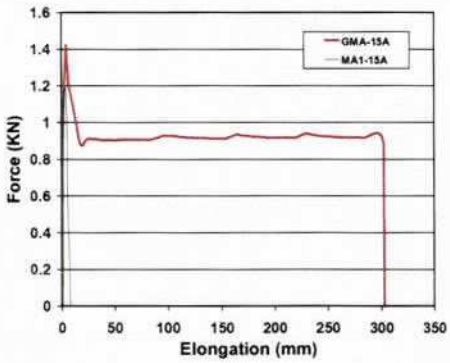

Fig. 5. Stress-strain curves for MA1-15A and GMA-15A.

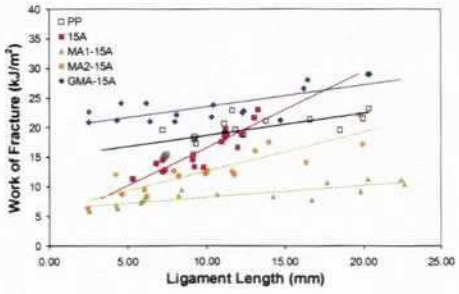

Fig. 6. Work of fracture as a function of ligament length for PP and its nanocomposites.